Proceedings of the 34th Scandinavian Symposium on Physical Acoustics, Geilo 30 January – 2 February, 2011.

MEASUREMENTS AND 3D SIMULATIONS OF ULTRASONIC DIRECTIVE BEAM TRANSMISSION THROUGH A WATER-IMMERSED STEEL PLATE

Kjetil Daae Lohne [1,2], Per Lunde [1,2], Magne Vestrheim [1]

[1] University of Bergen, Dept. of Physics and Technolgy, Allégaten 55, N-5007 Bergen, Norway.
[2] Christian Michelsen Research AS, P.O.Box 6031 Postterminalen, N-5892 Bergen, Norway.

Abstract

A 3D full-wave angular spectrum simulation model for reflection and transmission of ultrasonic directive circular piston sound fields, from and through a fluid-immersed isotropic solid plate has been implemented. Transmitted sound fields, frequency spectra and time-domain signals through a water-immersed steel plate have been studied theoretically with the 3D model and compared with experimental results for normal and oblique incident angles. Longitudinal and shear wave velocities for the steel plate have been determined from measured transmitted frequency response at normal incidence.

Contact author: Lohne, K. D., Christian Michelsen Research AS, P.O. Box 6031, NO-5892 Bergen, NORWAY, email: kjetil@cmr.no

1. Introduction

In applications involving transmission of ultrasonic signals through a plate or pipe wall, the acoustic properties of the transmitted field and signals may be highly important. Examples of non-invasive ultrasonic applications include e.g. non-invasive flow metering of oil and gas, hydrate/wax detection, monitoring of offshore petroleum separators, and non-destructive testing. Properties of importance may include signal level, bandwidth, signal-to-noise ratio, pulse form and directivity. Theoretical models for the transmission of ultrasonic directive beams through solid plates at normal and oblique incident angles which include description of such properties, may be valuable tools for constructing and optimizing instruments for these and other applications - especially if the ultrasonic directive beam is realistically described. For a fluid-immersed solid plate, the parameters influencing the transmission are e.g. the directivity, vibration pattern and operation frequency of the transducer in addition to the angle of incidence, material parameters and the thickness of the plate.

2D bounded beam reflection and transmission simulations using incident Gaussian beams have been studied by e.g. [1] - [9]. However, a 2D Gaussian beam without side lobes may not give a sufficiently realistic description of the 3D sound field radiated from a transducer in an experimental setup, and hence the interaction of the beam with the plate and the transmitted field and signals. Most of the works were also limited to resonance behaviours of the structure instead of using exact plane wave reflection and transmission coefficients, i.e. the solutions were only valid in the vicinity to excitation of Rayleigh-Lamb type of modes in the solid plate. 3D transmission for isotropic solid plates using a more realistic circular uniform piston source model combined with full-wave angular spectrum modelling have been studied in [10] - [12]. However, only a single frequency component was investigated and the works focused on nonlinear effects.

There is today a need for addressing and studying theoretically and experimentally the transmission with respect to signal properties in time, frequency and space when exciting Rayleigh-Lamb type of modes in the solid plate, using realistic simulations of the transmitter transducer. In the present work, a 3D full-wave angular spectrum simulation model for transmission of ultrasonic directive beams through a fluid-immersed solid plate has been implemented using a piston type of directive source, and transmitted fields and signals through a water-immersed steel plate have been studied theoretically and compared with experimental results with respect to acoustic properties. The work extends earlier work e.g. by enabling numerical study of the transmission of a directive circular piston sound field (with major lobe and side lobes) in time-space (signal shape), frequency-space (frequency spectra) and frequency-wave number domains, at arbitrary angles of incidence.

2. Simulation models

A plane wave simulation model and a 3D directive beam simulation model have been used in the present study. The plane wave model is important since it is incorporated into the 3D beam model and since it can be used for determining the wave velocities in the steel plate. In addition, the plane wave model is important since the dispersion curves and transmitted frequency spectrum shows when the Rayleigh-Lamb modes are excited and when maximum transmission is expected.

2.1 Plane wave model

Rayleigh-Lamb wave dispersion in an infinite isotropic elastic solid plate in vacuum is governed by the Rayleigh-Lamb frequency equations which were given in 1889 by Lord Rayleigh [13] and Lamb [14] and in 1917 by Lamb [15]. For an elastic solid plate, loaded with fluids at both interfaces, the modes inside the plate are termed leaky Rayleigh-Lamb waves. Leaky Rayleigh-Lamb waves are a function of the frequency, the thickness of the plate and the incident angle [16], [17].

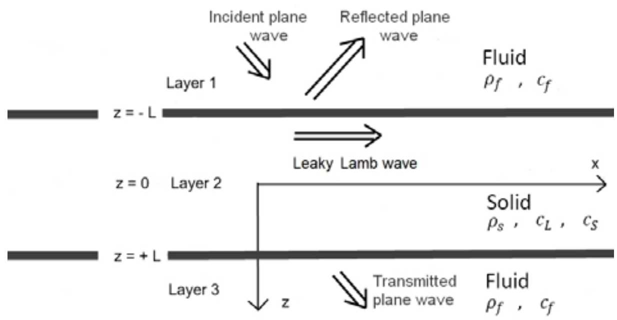

Figure 1. *Reflection and transmission of an infinite incident plane wave for a fluid-immersed solid plate.*

A plane wave model for a fluid-immersed solid plate can be established as a three-layer system where the layers have plane interfaces. A schematic figure of the setup is shown in Figure 1 where the solid plate is loaded with the same fluid at the two interfaces. A Cartesian coordinate system is chosen as shown in Figure 1, and the components of particle motion are confined to the plate normal and to the along-plate wave propagation directions, z and x-directions, respectively. It is assumed that the layers in the model are infinite in both x and y-directions, and also that the Rayleigh-Lamb waves have no particle motion or variation in the y-direction, thus SH-modes are excluded here. The solid plate thickness in the z-direction is $2L$, while both layers with fluids are considered as semi-infinite half-spaces. The characteristic properties for a lossless elastic, solid plate are the density, ρ_S, the longitudinal wave velocity, c_L and the shear wave velocity, c_S. The characteristic properties for a fluid are the density, ρ_f, and the longitudinal wave velocity, c_f.

The pressure reflection and transmission coefficients for incident plane waves in a system consisting of a fluid-immersed solid plate can be solved using a matrix method where the six equations resulting from the boundary conditions are collected into a single matrix equation. The matrix equation accounts for the boundary conditions (continuity of the normal displacement, u_z, continuity of normal stress, T_{zz}, and vanishing of the shear stress, T_{xz}) at both interfaces of the plate. For a fluid-immersed solid plate, the matrix can be reduced to two analytical expressions for the pressure reflection and transmission coefficients, R and T, respectively. These two coefficients are defined as the ratio of reflected and transmitted pressure amplitudes over incident pressure amplitude, respectively, and can be found by setting the incident plane wave amplitude equal to unity, e.g. as in [18],

$$R = i\frac{M^2 - N^2 + 1}{2M + i(M^2 - N^2 - 1)}\,, \qquad T = \frac{2N}{2M + i(M^2 - N^2 - 1)}\,, \tag{1}$$

where

$$N = \frac{\rho_S c_L \cos(\theta_f)\cos^2(2\theta_S)}{\rho_f c_f \cos(\theta_L)\sin(2hL\cos(\theta_L))} + \frac{\rho_S c_S \cos(\theta_f)\sin^2(2\theta_S)}{\rho_f c_f \cos(\theta_S)\sin(2kL\cos(\theta_S))}\,, \tag{2}$$

$$M = \frac{\rho_S c_L \cos(\theta_f)\cos^2(2\theta_S)}{\rho_f c_f \cos(\theta_L)\tan(2hL\cos(\theta_L))} + \frac{\rho_S c_S \cos(\theta_f)\sin^2(2\theta_S)}{\rho_f c_f \cos(\theta_S)\tan(2kL\cos(\theta_S))}\,, \tag{3}$$

and where h and k are the wave numbers for longitudinal and shear waves in the solid plate, respectively, θ_f is the angle of the incident, reflected and transmitted waves in the fluid, and θ_L and θ_S are the angle of longitudinal and shear waves in the solid plate, respectively. The reflection and transmission coefficients in Eq. (1) are for lossless plates if lossless material parameters are used in the equations, however, absorption may be taken into account by introducing complex wave velocities [12].

All higher order symmetric and antisymmetric Rayleigh-Lamb modes in a solid plate in vacuum have cut-off frequencies, i.e. only the zeroth-order symmetric and antisymmetric modes, S_0 and A_0 respectively, exist for very low frequencies. The cut-off frequencies for higher order Rayleigh-Lamb modes occur at specific frequency-thickness products where the horizontal phase velocity approaches infinity [16]. The cut-off frequencies for higher order symmetric Rayleigh-Lamb modes are given as [16],

$$f_n^S = \frac{c_S n}{2L}, \quad n = 1,2,3,\dots \quad , \tag{4}$$

$$f_m^S = \frac{c_L m}{4L}, \quad m = 1,3,5,\dots \quad , \tag{5}$$

respectively. The cut-off frequencies for higher order antisymmetric Rayleigh-Lamb modes are given as [16],

$$f_n^A = \frac{c_L n}{2L}, \quad n = 1,2,3,\dots \quad , \tag{6}$$

$$f_m^A = \frac{c_S m}{4L}, \quad m = 1,3,5,\dots \quad , \tag{7}$$

respectively. The resonance frequencies for a solid plate in vacuum can be expressed with the two equations for longitudinal and shear modes, $f_{L,p}$ and $f_{S,q}$, respectively. These two equations can be found by collecting Eqs. (5) and (6), and Eqs. (4) and (7), and are then given as,

$$f_{L,p} = \frac{c_L p}{4L}, \quad p = 1,2,3,\dots \quad , \tag{8}$$

$$f_{S,q} = \frac{c_S q}{4L}, \quad q = 1,2,3,\dots \quad . \tag{9}$$

The longitudinal and shear wave velocities can be determined from the resonances at the frequencies given in Eqs. (8) and (9), respectively. For a solid plate immersed in a fluid with low acoustic impedance compared to the solid, maximum transmission is almost equal to excitation of Rayleigh-Lamb modes for the same plate in vacuum, and the cut-off frequencies, $f_{L,p}$ and $f_{S,q}$, can be found from reflection or transmission when the incident ultrasonic plane wave approaches the normal incident angle.

2.2 Three-dimensional directive beam model

The interaction between a 3D ultrasonic directive beam and a fluid-immersed solid plate results in a reflected ultrasonic pressure field from the solid plate and a transmitted ultrasonic pressure field through the solid plate. Inside the plate, leaky Rayleigh-Lamb modes are generated at certain combinations of frequency and incident angle.

Landsberger [10], Landsberger and Hamilton [11] and Younghouse [12] used theoretical models based on the angular spectrum method to calculate 3D reflected and transmitted fields (spatial space domain) from and through a fluid-immersed solid plate. They were all interested in studying nonlinear effects associated with the interaction of an obliquely incident, finite amplitude ultrasonic beam with the fluid-immersed solid plate, to assess the potential for using immersion techniques to measure the nonlinear acoustical parameters for the solid plate. Their theoretical models account for the combined effects of diffraction, reflection, transmission and second harmonic generation in the fluid (weak nonlinearity, i.e.

plate nonlinearity has been considered to be negligible). Diffraction was modelled using the angular spectrum method, while reflection and transmission were modelled using plane wave reflection and transmission coefficients together in the angular spectrum method. Thermoviscous attenuation was accounted for in the fluid by using complex wave numbers while the solid plate was assumed to be lossless since aluminium has a fairly low absorption coefficient for the frequency investigated.

Reflection from and transmission through a solid plate which is thick compared to the ultrasonic pulse length was theoretically and experimentally examined in [10] and [11], thus internal reflections were ignored and simplified reflection and transmission coefficients were used in the calculations. The works in [10] and [11] were extended in [12] by considering an arbitrary thickness of the solid plate instead of a thick solid medium. Hence, multiple reflections inside the plate were accounted for by using exact plane wave pressure reflection and transmission coefficients for a fluid-immersed solid plate, and the model in [12] had valid solutions for arbitrary oblique incident angles. Reflections from and transmissions through a fluid-immersed solid plate were theoretically and experimentally examined by considering an obliquely incident diffracting ultrasonic beam. An angular spectrum method was used in [12] to include the diffraction of a bounded beam generated with a plane piston source, by applying a 2D Fourier transform to the spatial pressure distribution in a plane parallel to the plane of the solid plate, and 3D ultrasonic fields could be calculated.

The model implemented and presented here is based on basic physical equations presented as e.g. in [12] for a similar 3D beam model; That is, a piston source is used as transmitter, plane wave reflection and transmission coefficients for a fluid-immersed solid plate are used, and the angular spectrum method is used for extrapolating a pressure field from one plane to another plane. The full-wave 3D beam model implemented here is similar but also somewhat different from the model presented in [12]. Here, an analytical expression for the far-field pressure field from a baffled piston source at normal or oblique incidence is used to calculate the incident pressure field propagating towards the steel plate. This pressure field is calculated directly in a reference plane, which is parallel to the interface of the steel-plate. Another approach was used in [12] for calculating the incident pressure field, i.e. the source pressure distribution (over the radius of the source) was Fourier spatial transformed to determine the spatial source spectrum at the piston face, and the spectrum could be from a focused or unfocused piston source. For oblique incidence, the source spectrum in the model in [12] is rotated using a rotation matrix, and then propagated towards the plate using the propagation term in the wave number-frequency domain.

A schematic figure of the 3D beam model used here is shown in Figure 2 where the 3D ultrasonic directive beam is generated using a circular piston source where the motion of the transducer surface acts in unison and where the piston is surrounded by a motionless infinite baffle. The directive ultrasonic field radiating from the piston source is normal or obliquely incident towards the fluid-immersed isotropic solid plate and consists of a major lobe and side lobes. The centre of the piston source is located at the origin of a (x, y, z) Cartesian coordinate system as shown in Figure 2. The 3D sound field from the piston source propagates towards the solid plate where the interaction occurs, i.e. the incident field is reflected from and transmitted through the plate. The 3D beam model includes the description of nonspecular reflection and transmission effects which occurs at certain combinations of excitation frequency and incident angle. The angular spectrum method is used together with the exact plane wave pressure reflection and transmission coefficients from Eq. (1) to describe the 3D propagation and diffraction of the incident ultrasonic pressure field from the piston source, in addition to the reflected and transmitted ultrasonic pressure fields from through the fluid-immersed plate, respectively. In addition to the 3D pressure fields, the model calculates reflection and transmission frequency spectra and time domain signals, for arbitrary incident angles and for arbitrary thickness of the solid plate. All calculations of the incident beam are carried out in the far-field from the piston source and the media are defined as loss-less in the calculations. The 3D beam model can easily be extended to include loss in the fluid and solid media by defining complex wave velocities or wave numbers, however this has not been tested.

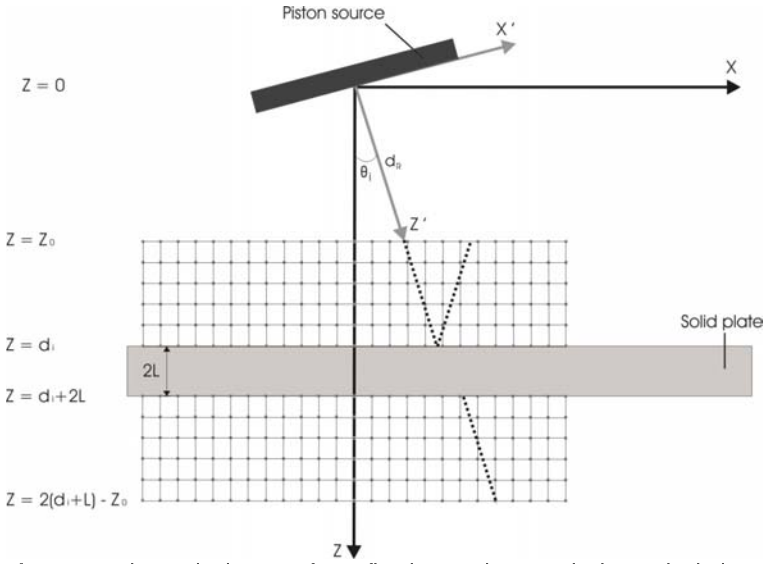

Figure 2. *Theoretical setup for reflection and transmission calculations with the 3D beam model where the ultrasonic bounded beam is generated with a piston source. A decimated example of the calculation grid for the incident and reflected field is shown only in two-dimensions here as dots from $z = z_0$ to $z = d_i$. The corresponding decimated calculation grid for the transmitted field is shown only in two-dimensions here as dots from $z = d_i + 2L$ to $z = 2(d_i + L) - z_0$.*

The incident angle between the piston source and solid plate is θ_i, and the distance between the centre of the piston source and the solid plate is d_i, thus the upper interface of the solid plate is positioned at $z = d_i$ in the coordinate system. The coordinate system is oriented such that the plate-thickness is along the z-axis, thus the x and y coordinates are in planes parallel to the interfaces of the solid plate, and the y-axis points out of the page. It is assumed that the piston source is rotated in the x- and z-directions while the y-direction is kept constant for an oblique incident beam, i.e. the piston source is rotated around the y-axis and the beam central axes are in the (x, z) plane. Another Cartesian coordinate system, (x', y, z'), follows the orientation of the piston source, i.e. this coordinate system is identical to the (x, y, z) Cartesian coordinate system at normal incidence. The (x', y, z') coordinate system has an y-axis which is identical to the original (x, y, z) coordinate system.

An example of the decimated calculation grid for the incident, reflected and transmitted ultrasonic fields in the x- and z-directions is shown in Figure 2, however, for 3D modelling there are also similar calculation points in the positive and negative y-direction, which are not shown in the figure. The schematic setup of the 3D beam model in Figure 2 shows that $d_i > z_0$ and that the calculation of the reflected field starts at $z = d_i$ and ends at $z = z_0$, the calculation of the transmitted field starts at $z = d_i + 2L$ and ends at $z = 2(d_i + L) - z_0$. The reference plane is defined to be the (x, y) plane at $z_{ref} = d_i$ for calculations of reflected and transmitted pressure fields, and the reference plane must be in the far-field from the piston source for normal and oblique incident angles. The far-field distance on the acoustic-axis of the piston source, i.e. on the z'-axis, is given by the Rayleigh distance. The reference plane at $z_{ref} = d_i$ for calculations of the reflected and transmitted pressure fields is chosen instead of $z_{ref} = z_0$ to reduce aliasing problems which may occur when extrapolating a reference field a long distance with the angular spectrum technique.

The numerical modelling of the diffraction and propagation of a monochromatic continuous wave field in the 3D beam model involves four steps which are described below.

1) The first step is the sampling of a 2D complex piston source pressure field, $p(x, y, z_{ref}, \omega)$, in the reference plane (x, y) at $z = z_{ref}$ over a grid of points which is parallel to the solid plate, but non-parallel to the face of the piston source for oblique incident angles. The pressure field is sampled in the far-field from the piston source, and the spatial distribution of the acoustic pressure, $p(x, y, z_{ref}, \omega)$, in the reference plane is calculated in the space-frequency domain.
2) The second step is to use a 2D spatial Fourier transform of the 2D reference pressure field from step (1), i.e. the pressure in the space-frequency domain, $p(x, y, z_{ref}, \omega)$, is transformed into the wave number-frequency domain to $P(h_{x,f1}, h_{y,f1}, z_{ref}, \omega)$ which is called the angular spectrum. Hence, the pressure field is decomposed into a 2D angular spectrum of plane waves which travel in different directions.
3) The third step is to multiply each point in the 2D angular spectrum of the reference pressure field, $P(h_{x,f1}, h_{y,f1}, z_{ref}, \omega)$, from step (2) by a propagation term, $e^{ih_{z,f1}(z-z_{ref})}$, and exact plane wave reflection or transmission coefficients in the spatial angular frequency domain, $R(h_{x,f1}, h_{y,f1}, \omega)$ and $T(h_{x,f1}, h_{y,f1}, \omega)$, using Eq. (1), where $h_{x,f1}$, $h_{y,f1}$ and $h_{z,f1}$ are the wave number components in the x, y and z directions in the fluid. The propagation term accounts for the phase change that each plane wave will undergo on its journey to the prediction plane while the exact plane wave reflection and transmission coefficients includes the interaction of the incident pressure field with the fluid-immersed solid plate.
4) The final step is to apply a 2D inverse spatial Fourier transform of the product from step (3) to yield the pressure field contour over the prediction plane in the space-frequency domain, $p(x, y, z, \omega)$.

The 3D beam model as described above in the four steps calculates the diffraction and propagation of the incident pressure field towards the solid plate and the diffraction and propagation of the reflected and transmitted pressure fields from the solid plate after the interaction with the solid plate. The calculation of the frequency spectrum in one prediction plane is carried out by following the four steps above for a range of frequencies. However, it is only necessary to calculate the reflected and/or transmitted field in one prediction plane, i.e. in a (x, y) plane for a given z.

The far-field pressure from a circular and uniform piston source in a rigid baffle of infinite extent can be calculated in the (x', y, z') coordinate system with the formula given by Schmerr [19] as

$$p(x', y, z', \omega) = -i\omega\rho_f a^2 v_0(\omega) \frac{J_1\left(h_f a \sin\theta\right)}{h_f a \sin\theta} \frac{e^{ih_f\sqrt{x'^2+y^2+z'^2}}}{\sqrt{x'^2 + y^2 + z'^2}}, \tag{10}$$

where θ is the angle between the point (x', y, z') and the centre of the piston source, a is the radius of the source, v_0 is the velocity on the surface of the source, and h_f is the wave number in the fluid. The pressure in Eq. (10) is in the 3D beam model calculated for (x', y, z') points which lies in the reference plane, i.e. the pressure, $p\left(x, y, z_{ref}, \omega\right)$, is calculated directly in the (x, y) plane at $z = z_{ref}$ by using Eq. (10). The reflected ultrasonic pressure field, p_R, from $z = d_i$ to $z = z_0$ and the transmitted ultrasonic pressure field, p_T, from $z = d_i + 2L$ to $z = 2(d_i + L) - z_0$ in the space-frequency domain are calculated using Eqs. (11) and (12),

$$p_R(x, y, z, \omega) = \frac{1}{4\pi^2} \iint_{-\infty}^{+\infty} \mathcal{H}_R e^{i(h_{x,f1}x + h_{y,f1}y)} dh_{x,f1} dh_{y,f1} \quad , \tag{11}$$

$$p_T(x, y, z, \omega) = \frac{1}{4\pi^2} \iint_{-\infty}^{+\infty} \mathcal{H}_T e^{i(h_{x,f1}x + h_{y,f1}y)} dh_{x,f1} dh_{y,f1} \quad , \tag{12}$$

where $\mathcal{H}_R$ and $\mathcal{H}_T$ are defined as,

$$\mathcal{H}_R = P\left(h_{x,f1}, h_{y,f1}, d_i, \omega\right) R\left(h_{x,f1}, h_{y,f1}, \omega\right) e^{ih_{z,f1}|z-d_i|} \quad , \tag{13}$$

$$\mathcal{H}_T = P\left(h_{x,f1}, h_{y,f1}, d_i, \omega\right) T\left(h_{x,f1}, h_{y,f1}, \omega\right) e^{ih_{z,f1}|z-2L-d_i|} \quad , \tag{14}$$

respectively. The 2D pressure reflection and transmission coefficients, $R\left(h_{x,f1}, h_{y,f1}, \omega\right)$ and $T\left(h_{x,f1}, h_{y,f1}, \omega\right)$, are calculated in the wave number-frequency domain using Eq. (1).

The calculation of time domain signals somewhere in the reflected or transmitted field is carried out by:

- First finding the frequency spectrum at this point in the reflected or transmitted field.
- Then the frequency spectrum is multiplied with a time-frequency Fourier transformed source signal.
- The product is transformed into the time domain by applying an inverse time-frequency Fourier transform.

The input time domain signal ("source signal") in the 3D beam model can in general be a synthesized or measured signal. Measured monochromatic burst signals at different frequencies have been used as input to the 3D beam model in the results presented here. These signals have been recorded with the measurement setup and is the signals which are measured in water at $z = d_i$ with the plate absent when $\theta_i = 0$, i.e. the incident signal at the upper interface of the plate on the acoustical axis of the transducer for a normal incident beam.

3. Experimental and simulation setups

The experimental setup for measuring transmission through a water-immersed steel plate is shown in Figures 3 and 4, where a 6.05 mm thick, 50 cm wide and 76 cm high AISI 316L stainless steel plate is mounted in the middle of a 60 cm wide, 60 cm high and 150 cm long water-filled tank. Sound-fields could be automatically measured in a plane parallel to the steel plate at different distances from the plate with the setup shown in Figure 4.

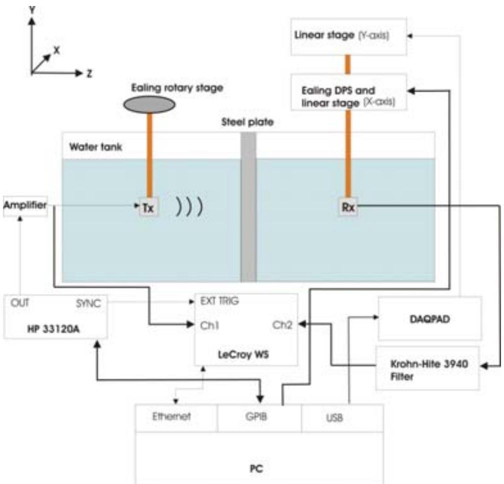

Figure 3. Schematic figure of the measurement setup.

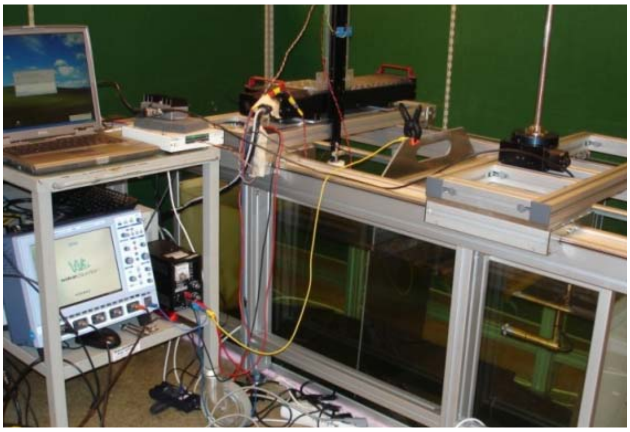

Figure 4. Photography of the measurement setup.

A Panametrics V301 0.5 MHz transducer and a 1 mm needle calibrated PVDF probe hydrophone (PA-407) manufactured by Precision Acoustic Limited were used as transmitter and receiver transducers, respectively. The incident angle between transmitter and plate was controlled with an Ealing rotary stage. A computer controlled the HP 33120A function generator that generated the transmitted signal, and a 20 dB Apex amplifier was used between the signal generator and transmitter transducer. The vertical and horizontal position of the hydrophone, the rotary stage and the data collection on a LeCroy Wavesurfer 424 oscilloscope were also controlled with a computer. An Ealing linear stage was used to scan the transmitted sound-field with the hydrophone in the horizontal direction, and a specific system was used to scan the transmitted sound-field with the hydrophone in the vertical direction. The resolutions used in the measurements were 1 mm in both the horizontal and vertical directions. On the receiver side, the sound-fields were measured with the PA-407 hydrophone. The measured signals were taken through a 3940 Krohn-Hite bandpass-filter and amplified with 40 dB. Sinusoidal burst signals with a length of 60 periods were used in all measurements (except for the results shown in Figures 9 and 10) to excite the transmitter transducer. The amplitudes of the received signals were measured as a mean of three periods around the 48th cycle, 50 pulses were averaged at the oscilloscope, and the frequencies region of interest was 350 kHz - 800 kHz.

Transmission measurements and 3D beam model simulation results are presented in Section 4 and have been carried out with the centre of the transducer front positioned at $z = 0$ mm, with the upper interface of the steel plate positioned at $z = d_i = 270$ mm, and with the hydrophone/receiver point positioned at $z = 2(d_i + L) - z_0 = 376.05$ mm, i.e. 100 mm from the steel plate in the z-direction (cf. Figure 2). The measurement results presented here were carried out at $y = 0$, and the simulation results with the 3D beam model here are also only presented at $y = 0$ for comparison. In the 3D beam model simulation results the calculation points in the x and y -directions have been from -500 mm to +500 mm, with 1024 points in each direction, i.e. with a sampling interval of 976.56 μm. The minimum and maximum horizontal wave number have been -30.9833 m^{-1} to 4368.3535 m^{-1}, respectively

All transmission measurements and simulation results with the 3D beam model have been normalized with a normalization method where the transmitted pressure at arbitrary incidence, $p_{tra}(x, y = 0, z, f, \theta_i)$, at $z = 2(d_i + L) - z_0$, are divided by the incident pressure, $p_{inc}(x, y = 0, z, f, \theta_i = 0°)$, in water with the plate absent at the position $(x, y, z) = (0,0, d_i)$. The incident pressure in water that is used as a normalization factor was measured/calculated at normal incidence, i.e. when $\theta_i = 0°$. Hence, the formula for the normalization of measurements and simulations with the 3D beam model is given as

$$p_{norm}(x, 0,2(d_i + L) - z_0, f, \theta_i) = \frac{p_{tra}(x,0,2(d_i+L)-z_0,f,\theta_i)}{p_{inc}(0,0,d_i,f,0°)} . \tag{15}$$

Simulation results presented from the plane wave model are the pressure transmission coefficients from Eq. (1), i.e. the normalization factor is equal to one. Material data used in the simulations (if else not specified) are given in Table 1. The density of the AISI 316L stainless steel is taken from [20] and the longitudinal and shear velocities have been determined in [21] and as shown in Section 4.4. The characteristic properties for water are taken from [17].

Table 1. *Characteristic properties for media used in the simulations.*

Material	Density [kg/m^3]	Longitudinal wave velocity [m/s]	Shear wave velocity [m/s]
AISI 316L stainless steel	8000	5780	3130
Water	1000	1483	

4. Results

Transmitted sound fields, frequency spectra and time-domain signals through a water-immersed steel plate have been studied theoretically with the 3D beam model and compared with experimental results at normal and oblique incident angles. In addition, longitudinal and shear wave velocities have been determined from measured transmitted frequency response at normal incidence through the steel plate.

4.1 Measurement of the transducer directivity in water

Directivities for the 0.5 MHz Panametrics V301 transducer were measured in water at different frequencies and compared to piston source simulations, using Eq. (10), as shown in Figure 5. The simulation results in Figure 5 were calculated using the effective radius $a = a_{eff}$, calculated from the measured directivity at 500 kHz using the measured beam-width, $2\theta_{-3dB}$, for the main lobe. The beam-width is defined as the width where the sound pressure level of the main lobe is -3 dB down from the maximum level. The maximum level is at the acoustic axis and the beam-width is then given as $2\theta_{-3dB} \approx 2\sin^{-1}\left(1.616/h_f a_{eff}\right)$. The measured directivity at 500 kHz, results in $a_{eff} = 12.90$ mm.

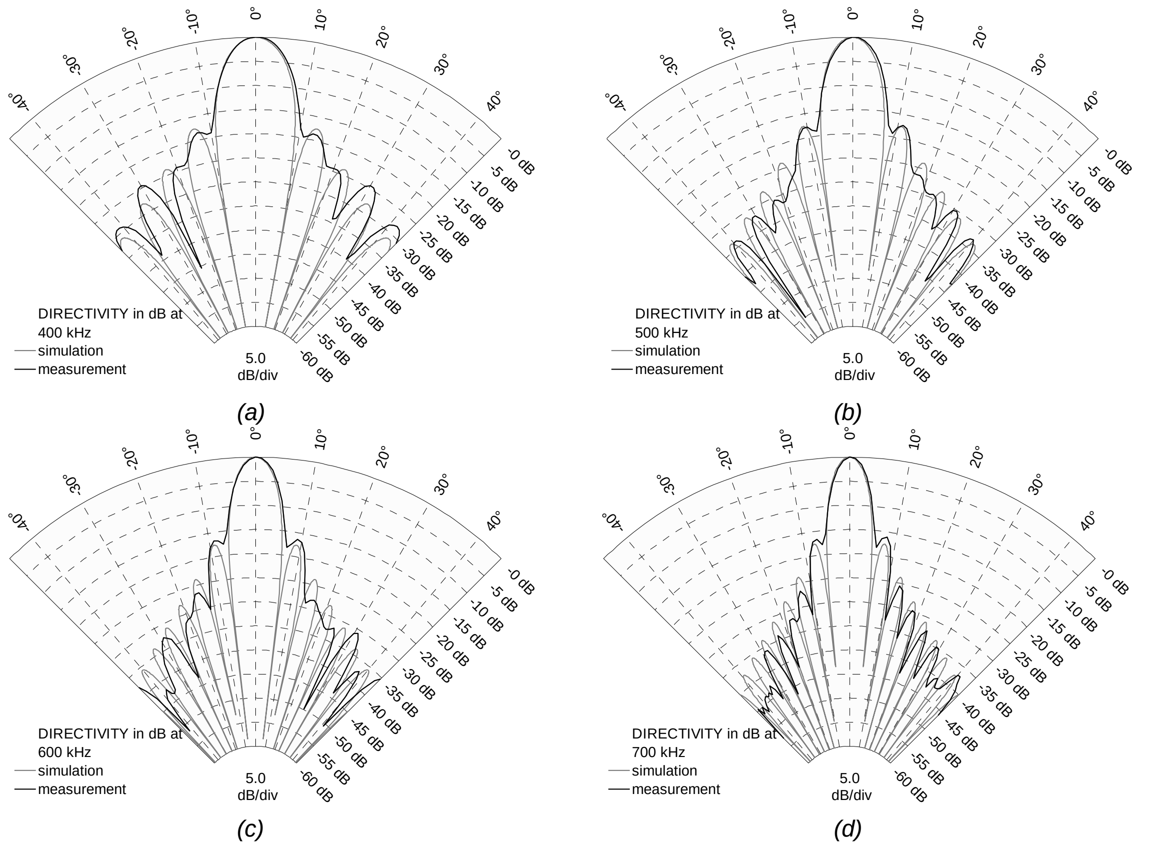

Figure 5. *Measured and simulated directivities at (a) 400 kHz and ka = 21.86, (b) 500 kHz and ka = 27.33, (c) 600 kHz and ka = 32.79, (d) 700 kHz and ka = 38.26.*

The results in Figure 5 (a) – (d), show that the piston model simulation describes the main lobe very well at different frequencies. However, the side lobes are not accurately described with the piston model, especially at low frequencies. This may affect the accuracy in the 3D beam model where the piston source is used to model the transmitter transducer, especially at oblique incidences.

4.2 Simulation result with plane wave model

A plane wave simulation result, using Eq. (1), of the pressure transmission coefficient for the 6.05 mm thick steel plate in water is shown in Figure 6 for various frequencies and incident angles. The dispersion curves for Rayleigh-Lamb modes in the steel plate in vacuum are plotted on top of the transmission plot in Figure 6 as black curves, and are labelled as symmetric and antisymmetric Rayleigh-Lamb modes after Eqs. (4) – (5) and Eqs. (6) – (7), respectively.

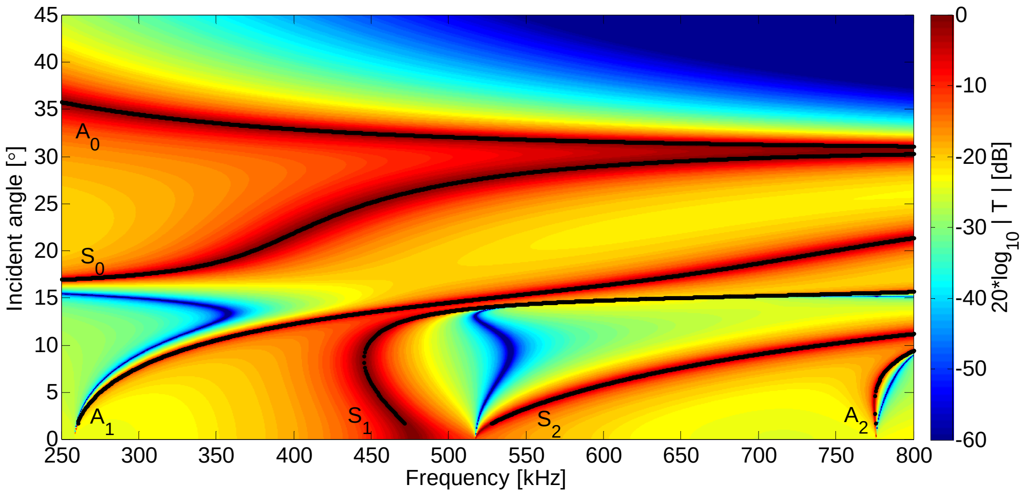

Figure 6. *Spectrum of the pressure transmission coefficient for the water immersed and 6.05 mm thick steel plate, calculated with the plane wave model as a function of frequency and incident angle. The black curves on top of the pressure transmission spectrum are the dispersion curves for Rayleigh-Lamb modes in the steel plate in vacuum.*

The plane wave simulation result of the pressure transmission coefficient in Figure 6 shows that for a water-immersed steel plate, the maximum transmission corresponds to the dispersion curves for a steel plate in vacuum, i.e. maximum transmission occurs when Rayleigh-Lamb waves are excited in the steel plate.

4.3 Measurement of the transducer frequency response in water and through the plate

The frequency response of the Panametrics V301, 0.5 MHz transducer was measured in water with the plate absent, and recorded with the hydrophone on the acoustical axis ($x = 0, y = 0$) at $z = 376.05$ mm. A reflection problem (interference in measured signals) was discovered from the hydrophone when using long excitation signals in the measurement. The reflection was caused by an edge 26 mm from the tip of the needle hydrophone. Several mechanical methods were attempted to reduce this problem and some of the tested methods reduced the problem to some extent, but not significantly enough in order to compare measurements and simulations. The reflection is clearly visible in the transducer frequency response in water as shown in the black curve in Figure 7. Two different normalization methods for the measurement is shown in Figure 7, i.e. the black curve is the measurement normalized with the maximum measured pressure in the frequency response, and the red curve is the measurement normalized using the normalization method presented in Section 3, respectively. In the normalization method, the measured frequency response in water at $z = 376.05$ mm has been normalized with the frequency response to the transducer in water at $z = 270$ mm. The frequency response to the piston source in water at $z = 376.05$ mm is also shown in Figure 7 (blue curve), and the results is also normalized with the frequency response for the piston source in water calculated on the acoustical axis at $z = 270$ mm.

Figure 8 displays measured and simulated (with 3D beam model) transmitted frequency responses through the steel plate at normal incidence, on the acoustical axis $(x = 0, y = 0)$ and at $z = 2(d_i + L) - z_0 = 376.05$ mm. The same two normalization methods as used for the measurement in Figure 7 are applied to the measurement shown in Figure 8, i.e. the measurement is normalized to maximum measured transmitted frequency response (black curve) and to the frequency response to the transducer in water at $z = 270$ mm (red curve). A 3D beam model result of the transmitted frequency response recorded at $z = 2(d_i + L) - z_0 = 376.05$ mm is also shown in Figure 8 (blue curve), where the result is normalized with the frequency response to the piston source in water calculated at $z = 270$ mm.

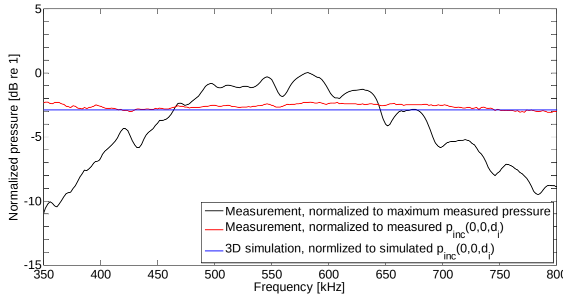

Figure 7. *Transducer response in water, measured and simulated with the 3D beam model. The measurement is normalized to maximum pressure (black curve) and with the normalization method (red curve). The 3D simulation is normalized with the normalization method.*

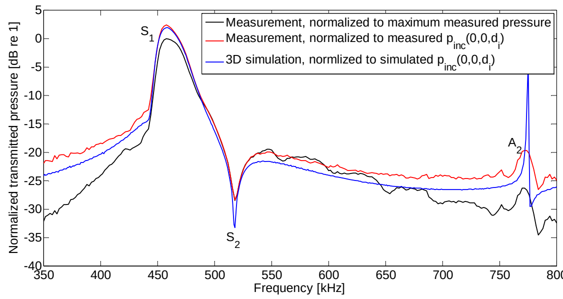

Figure 8. *Transmitted frequency response, measured and simulated with the 3D beam model. The measurement is normalized to maximum pressure (black curve) and with the normalization method (red curve). The 3D simulation is normalized with the normalization method.*

The results presented in Figure 7 show the benefit of using the normalization method, i.e. the reflection problem in the recorded signals (in water) with the hydrophone is significantly reduced (no significantly “ripples”), the measured frequency response is also almost flat from 350 kHz to 800 kHz and the 3D beam model results can be directly compared to the measurement results since the transmission level at one frequency can be directly compared to the transmission level at another frequency even if the source sensitivity of the transmitter transducer at these two frequencies are different. The reflection problem (interference in measured signals) is also visible as shown in the black curve above 525 kHz in Figure 8 when normalizing the transmitted frequency response measurement with the maximum pressure in the frequency response, hence Figure 8 supports the use of the normalization method as can be seen in the measurement (red curve compared to black curve) above 525 kHz.

As mentioned in Section 2.2, the input time domain signal in the 3D beam model is measured monochromatic burst signals at different frequencies. These signals are the measured signals used for normalizing the result (red curve) presented in Figure 7, i.e. the incident signals in water at $z = d_i$. A benefit by using these measured time domain signals (at different excitation frequencies) in the 3D beam model is that these signals include the reflections that originates 26 mm from the tip of the needle of the hydrophone. Thus, by using measured signals in the 3D beam model, a better comparison of the simulated transmitted signals with measured transmitted signals is expected compared to using synthesized signals in the 3D beam model.

4.4 Determination of longitudinal and shear wave velocity

Measurements of ultrasonic backscattered reflection signals from and transmission signals through the water immersed steel plate are here used for determining c_L and c_S of the plate. These properties are together with the thickness and the density important inputs to the plane wave and 3D beam models. The longitudinal wave velocity can determined from backscattered reflection measurements at normal incidence. For a steel plate, it may be assumed that the longitudinal wave velocity is constant as a function of frequency, i.e. non-dispersive, e.g. in the frequency range from 350 kHz to 800 kHz. One technique is to use a signal which is shorter than twice the thickness of the solid plate and detection of transit times when the thickness of the plate is known. A 5 MHz Panametrics transducer with nominal element size diameter of 19 mm was used as both transmitter and receiver in such a measurement, a broadband pulse excitation was used in the measurements and zero-cross detection in the time-domain between different internal reflections in the steel plate showed that the longitudinal velocity for the steel plate is approximately 5780 m/s. For more information about the method, please refer to [21].

Another method for determination of the longitudinal wave velocity is the amplitude spectrum method that can be applied on both long and short signals. In the amplitude spectrum method, received signals are converted to the frequency domain using a fast Fourier transform. For plane waves at normal incidence, the plane wave theory shows that longitudinal modes in the steel plate are generated in the steel plate at different cut-off frequencies as shown in Eq. (8), which corresponds to maximum transmission and minimum reflection. However, since the beam from the transducer does not generate a pure and plane wave front incident on the steel plate, other modes in the plate may also be present and have impact on the longitudinal modes. Hence, this method may be accurate for some frequencies, but the method should be used in combination with a 3D beam model in addition to the plane wave model such that it can be verified that the specific modes can be used for accurately determination of the longitudinal wave velocity.

The normalized amplitude spectrum of a transmitted broadband signal through the water-immersed steel plate is shown in Figures 9 and 10. The 5 MHz transducer was used as transmitter in this measurement, a broadband pulse excitation was used, the hydrophone was used as receiver, and the beam from the transducer was normally incident towards the steel plate. A normalized 3D beam simulation result at normal incidence and a plane wave simulation result at 1° incidence are also shown in Figures 9 and 10 with the same configuration.

From Figures 9 and 10, there is found a fair agreement between the measured and simulated longitudinal resonance modes, except for the S_1 mode where the resonance peak in the plane wave simulation is at a higher frequency. In addition to the longitudinal modes, the measurement and 3D simulation result at normal incidence also displays some of the shear modes, and these may be used for determination of the shear velocity as will be shown later. Calculated longitudinal velocity from the longitudinal resonance peaks in the measurement shown in Figures 9 and 10 is given in Table 2.

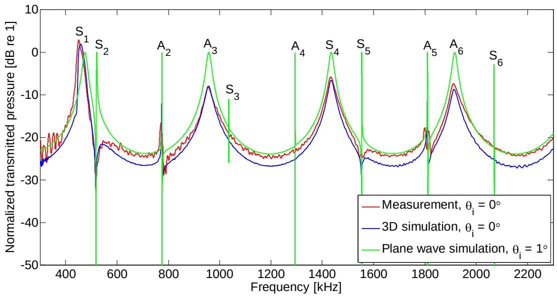

Figure 9. *Measured and 3D simulated transmitted frequency response at normal incidence (normalized with normalization method presented in Section 3), compared to plane wave simulation result at 1° incidence.*

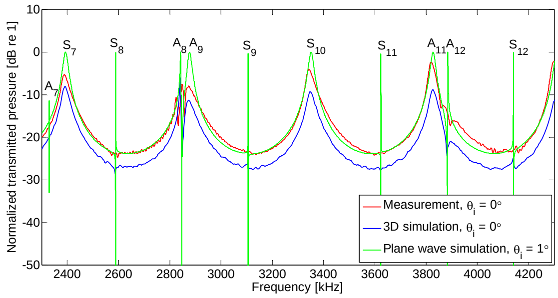

Figure 10. *As in Figure 9 but from 2300 kHz to 4300 kHz.*

Table 2. *Calculations of longitudinal wave velocity using Eq. (8) from the longitudinal resonance peaks in the measurement in Figures 9 and 10.*

p	Mode	$f_{L,p}$ [kHz]	c_L [m/s]	p	Mode	$f_{L,p}$ [kHz]	c_L [m/s]
1	S_1	451.1	5458.3	6	A_9	2874.4	5796.7
2	A_3	955.5	5780.8	7	S_{10}	3343.1	5778.8
3	S_4	1433.5	5781.8	8	A_{11}	3820.4	5778.4
4	A_6	1912.1	5784.1	9	S_{13}	4298.7	5779.4
5	S_7	2388.9	5781.1				

The results in Table 2 also indicate that for the 6.05 mm thick steel plate, a reasonable value for the longitudinal wave velocity seems to be approximately 5780 m/s. However, the S_1 and A_9 modes give different results. A small deviation is shown for the A_9 mode and may be due to the close presence in frequency of the A_8 mode. A large deviation is shown for the S_1 mode and the mode is not as symmetrical around the peak as the other modes. This may be explained due to the nature of this mode as can be seen in Figure 6, i.e. at small incident angles this mode exists at lower frequencies than it does at normal incidence, and this may shift the resonance peak downwards in frequency. In addition, the ultrasonic beam is less narrow at this frequency which results in a broader excitation area.

A normalized transmission measurement at normal incidence of the frequency response from 350 kHz to 800 kHz is shown in Figure 11 and compared to a plane wave simulation of the pressure transmission using Eq. (1) at normal incidence. Mono-chromatic burst signals were used in the transmission measurements in Figure 11, and the amplitude of the received signals was averaged from three periods around the 48 cycle. This measurement is the same as the measurement shown in Figure 8.

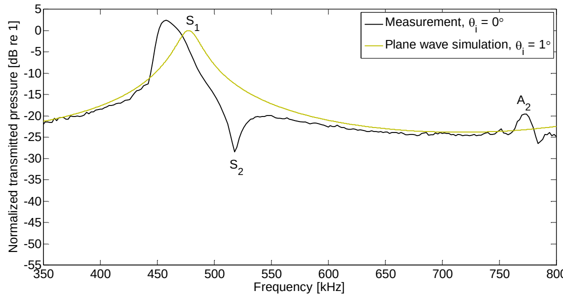

***Figure 11.** Measured transmitted frequency response at normal incidence (normalized with normalization method presented in Section 3) and compared to plane wave simulation result of pressure transmission coefficient at normal incidence.*

The maximum transmission in the measurement in Figure 11 is at 458 kHz, and is related to the first symmetric Lamb mode, S_1. As can be seen from Figure 11, only this mode is excited in the plane wave model at normal incidence, but the frequency of maximum transmission of S_1 in the plane wave simulation deviates from the measurement, and is located at 477.69 kHz. The same mismatch between measurement and plane wave simulation was shown in Figure 9 for this mode. The minimum measured transmission in Figure 11 is at 518 kHz, and is related to the second symmetric Lamb mode, S_2. The S_2 mode may be used to determine the shear velocity in the steel plate since the minimum value is well defined. The last maximum in the measurement in Figure 11 is around 773 kHz and is the second antisymmetric Lamb mode, A_2. This mode could also have been used to determine the shear velocity, but the peak is not as sharp and accurately defined as the minimum at 518 kHz.

Two 3D simulation results of the normalized transmitted pressure frequency response at normal incidence are shown in Figure 12 together with two plane wave simulation results of the pressure transmission coefficient using 0.2° incident angle. A longitudinal velocity of 5780 m/s was used in the four simulations in Figure 12, and two different shear velocities, 3130 m/s and 3050 m/s, were used. Figure 13 is identical to Figure 11, but a 3D simulation at normal incidence simulated using $c_S = 3130$ m/s, and a plane wave simulation at 1° incidence simulated using $c_S = 3130$ m/s are also included.

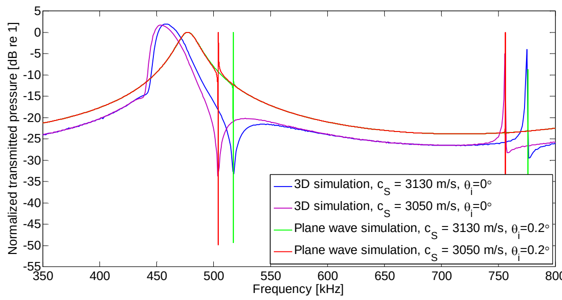

***Figure 12.** Simulations using two different shear velocities. 3D simulation results of normalized transmission through a water-immersed steel plate at 0° incidence, compared to two plane wave simulation results of pressure transmission coefficient at 0.2° incidence.*

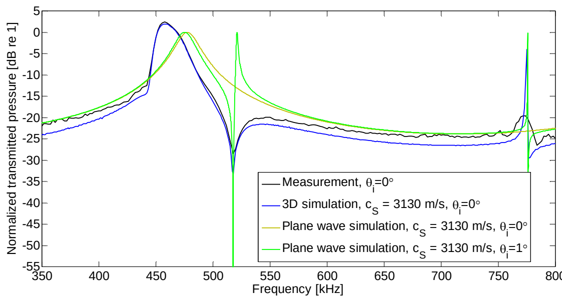

***Figure 13.** Comparison between normalized 3D simulation result and normalized measurement result of transmission through a water-immersed steel plate at 0° incidence. Results compared to plane wave simulation results of transmission coefficient at 0° and 1°.*

The two plane wave simulations in Figure 12 show that the S_1 mode is not notably affected by changing the shear velocity, but the S_2 and A_2 modes changes significantly. The same conclusions can be drawn from the 3D simulations in Figure 12 even if the S_2 is shifted approximately 4 kHz. The frequency of minimum transmission at the S_2 mode in the two 3D and two plan wave simulations in Figure 12 are summarized in Table 3, where Eq. (9) has been used to calculate the shear velocity from the cut-off frequency. Figure 12 show that the S_2 mode in the two plane wave simulation results follows the minimum transmission in the two 3D simulation results. The frequency resolution in the two 3D simulation results is 1 kHz, and the frequency resolution in the two plane wave results is 0.01 kHz. Hence, there are some small deviations in detected frequencies of minimum transmission, and hence in the calculated shear velocities. However, it seems like the shear velocity can be determined from a measurement of the minimum transmission at the S_2 mode, if the frequency resolution in the measurement is not to course.

Table 3. *Minimum frequencies determined from the simulations in Figure 12, and calculated shear velocities from these frequencies using Eq. (9), assuming they are the cut-off frequency for the second symmetric mode.*

Simulation model	Shear velocity used in simulation [m/s]	Frequency of minimum transmission [kHz]	Calculated shear velocity from minimum transmission [m/s]
3D beam model	3050	504	3049.2
	3130	518	3133.9
Plane wave model	3050	504.15	3050.1
	3130	517.36	3130.0

The 3D simulation results in Figure 13 shows a much better correlation to the measured result for the S_1 mode compared to the plane wave simulation results shown in Figures 12 and 13. It is also observed that both the normalized measurement and normalized 3D simulation of the transmission at the S_1 mode is above 0 dB, i.e. the transmitted signal is stronger than the incident signal.

Since the plane wave simulation results of the transmission at 0.1° incident angle, is both close to the cut-off frequency and to the 3D simulation results at normal incidence for the S_2 mode, this mode may be used for determining the shear velocity if the 3D beam model is accurate compared to the measured transmitted frequency spectrum. As shown in Figure 13, the measurement and the 3D simulation results of the transmitted frequency spectrum agree well when the longitudinal velocity is equal to 5780 m/s, and when the shear velocity equals 3130 m/s. Hence, the shear velocity in the steel plate is taken to be 3130 m/s.

4.5 Simulation results with 3D beam model

Normalized transmitted pressure frequency spectra, p_{norm}, simulated with the 3D beam model at different incident angles are shown in Figure 14 at $y = 0$, at $z = 2(d_i + L) - z_0$, for frequencies between 300 kHz and 800 kHz, and as function of the x-position.

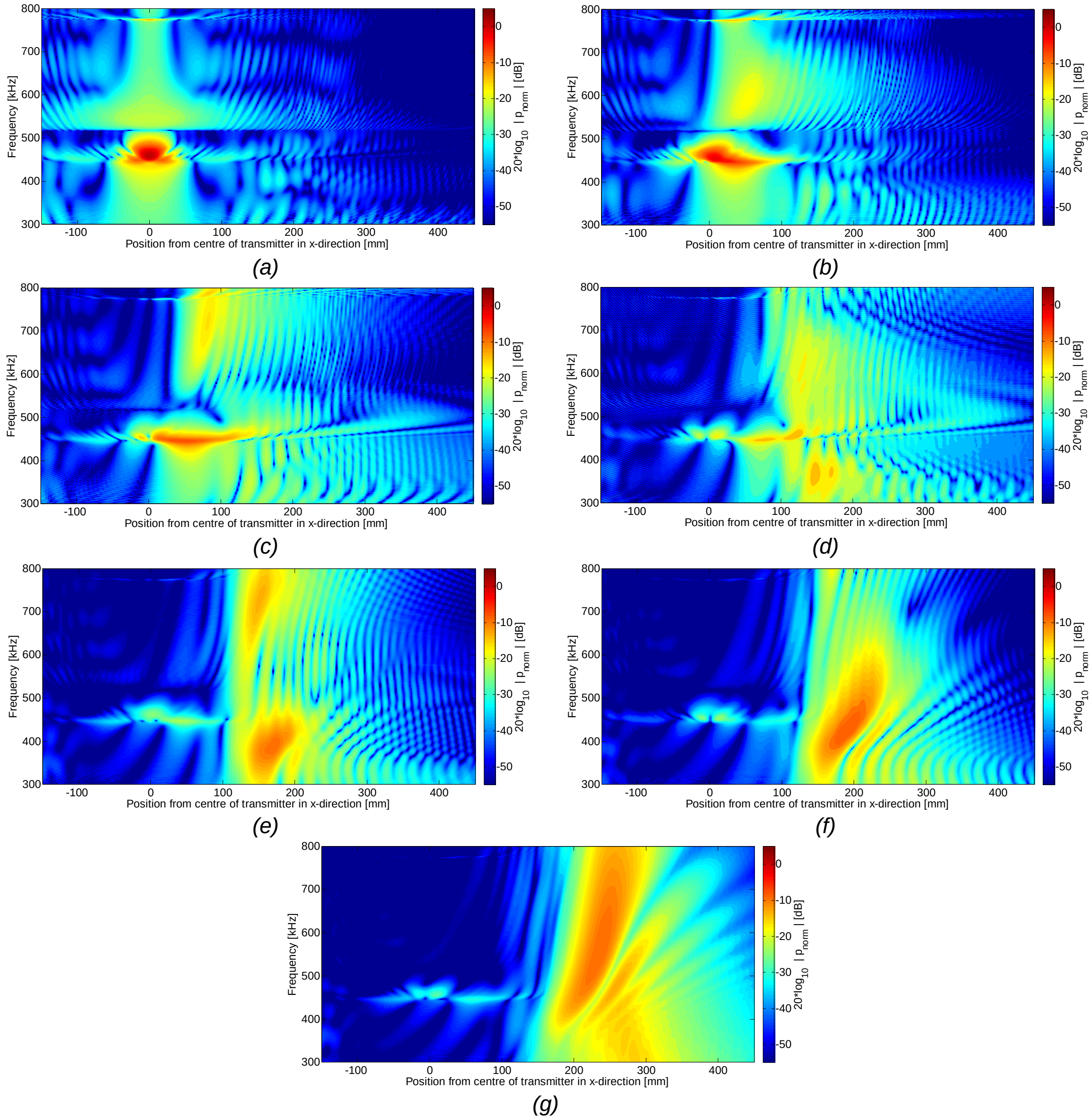

Figure 14. Simulated normalized transmitted pressure frequency spectra, using the 3D beam model, as function of the x-position at y = 0 mm, at z = 100 mm from the plate, and at the following incident angles (a) 0°, (b) 5°, (c) 10°, (d) 15°, (e) 20°, (f) 25°, (g) 30°.

The 3D simulation results presented in Figure 14 show that the transmission level is much lower at some incident angles, e.g. at 15° as shown in Figure 14 (d). In addition, it can be observed that the bandwidth (as a function of frequency) seems to be large for some incident angles, e.g. 25° and 30°, for a range of positions from the centre of the transmitter transducer. According to Figures 6, the bandwidth at 25° and 30° in Figure 14 is a result of the S_0 and A_0 modes. From Figure 14 it can be observed that the bandwidth is quite narrow when the incident angle is in the range from 0° to 15°.

From Figures 6 and 14 it is noted that:

- The region of maximum transmission at 0° in Figure 14 (a) corresponds to excitation of the S_1 mode (below 500 kHz), and the small maximum of transmission just below 800 kHz in Figure 14 (a) is the excitation of the A_2 mode. The S_2 mode is also visible as the distinct shift (not maximum) just above 500 kHz.
- The region of maximum transmission at 5° in Figure 14 (b) corresponds to excitation of the S_1 mode (below 500 kHz), and the small maximum of transmission just below 800 kHz in Figure 14 (b) is the excitation of the A_2 mode. In addition, there is a weak region of "maximum" transmission in Figure 14 (b) around 600 kHz, corresponding to the excitation of the S_2 mode and an apparent dip minimum between S_1 and S_2 modes. The same also applies for 10° in Figure 14 (c), but the S_2 mode is excited at a higher frequency, i.e. at 700 - 800 kHz, and the A_2 mode is outside the frequency range considered. According to Figure 6, the A_2 mode should have been present between 300 kHz and 350 kHz at 10°.
- The region of maximum transmission at 15° in Figure 14 (d) below 400 kHz most likely corresponds to excitation of the S_0 mode, while the region of maximum transmission for frequencies above 400 kHz is possibly the excitation of the combined S_1 and A_1 modes.
- The region of maximum transmission at 20° in Figure 14 (e) below 450 kHz corresponds to excitation of the S_0 mode, while the maximum transmission at about 650 – 800 kHz is the excitation of the A_1 mode.
- The region of maximum transmission at 25° in Figure 14 (f) centered at about 450 kHz, corresponds to excitation of the S_0 mode.
- The region of maximum transmission at 30° in Figure 14 (g) centered at about 600 kHz, corresponds to excitation of the A_0 mode, and the combination of the A_0 and S_0 modes.

4.6 Comparison of 3D simulation and measurement results

In the following, the normalized simulation results with the 3D beam model shown in Figure 14 are compared to normalized measurements at different incident angles. Figure 15 shows simulation results of normalized transmitted pressure sound fields, p_{norm}, compared to measurements at different positions in the x-direction (spatial distribution) for various frequencies and for 0°, 5°, 10°, 20°, 25° incident angles. Figure 16 shows simulation results of normalized transmitted pressure sound fields, p_{norm}, compared to measurements at various positions in the x-direction and for different frequencies (frequency responses) at various positions in the x-direction and for 0°, 5°, 10°, 25°, 30° incident angles. Simulation results of transmitted signals are compared to measurements at 0° incident angle and at $x = 0$ mm, at 10° incident angle and at $x = 0$ mm, and at 20° incident angle and at $x = 190$ mm, in Figures 17 - 19, respectively. The simulations shown in Figures 17 – 19 are normalized with the measured incident signals that are used in the 3D beam model.

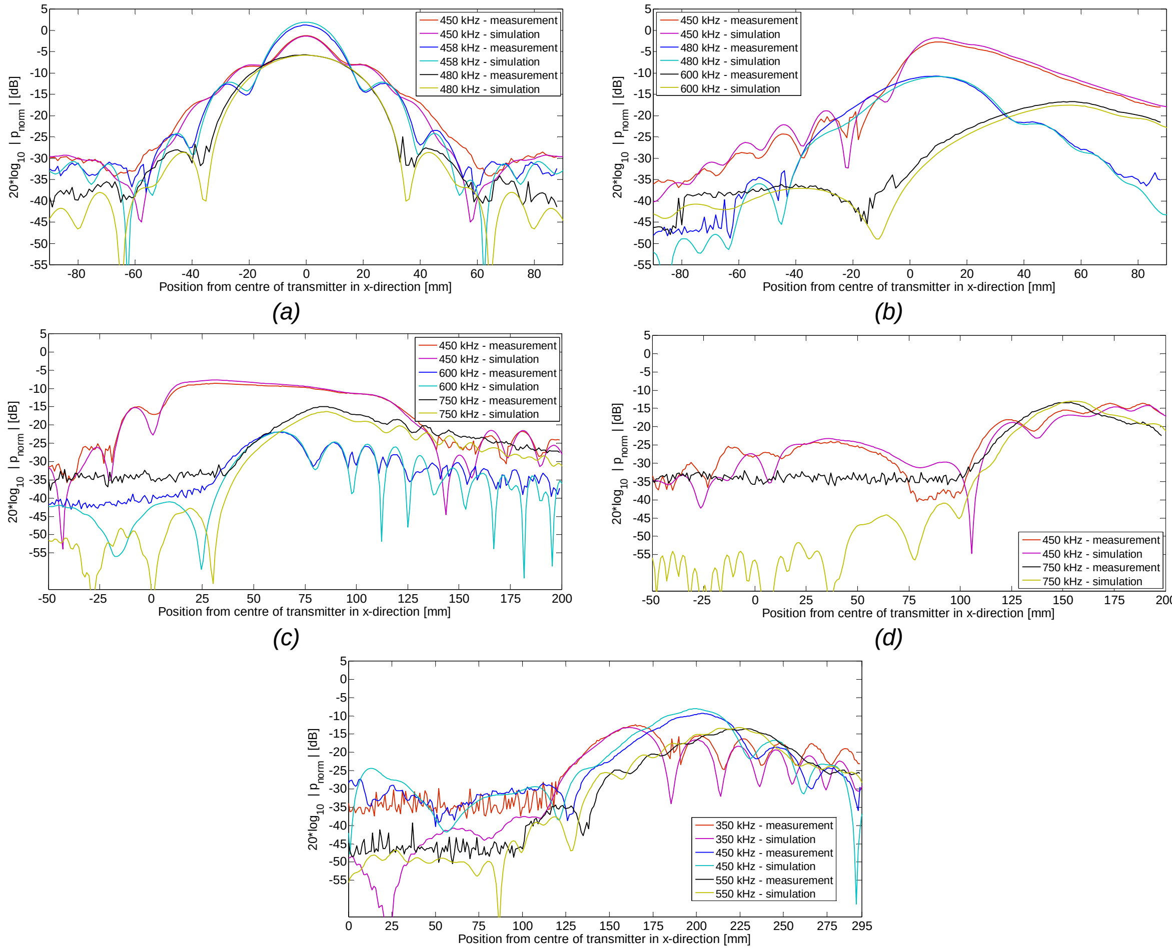

Figure 15. Measurement results and simulation results with 3D beam model of transmitted field at z=376.05 mm and y=0 mm. (a) 0° incident angle, for 450 kHz, 458 kHz and 480 kHz, (b) 5° incident angle, for 450 kHz, 480 kHz and 600 kHz, (c) 10° incident angle, for 450 kHz, 600 kHz and 750 kHz, (d) 20° incident angle, for 450 kHz and 750 kHz, (e) 25° incident angle, for 350 kHz, 450 kHz and 550 kHz.

From the simulation and measurement results shown in Figure 15 it is found that the simulations using the 3D beam model are in fair agreement with the measurement results for the main lobe and side lobes, at all frequencies and angles of incidence investigated. In some of the measurements, such as above 5° incidence, there is noise in the measurements of the side lobes which makes it difficult to compare the simulation results to the measurements. For the main lobe and higher side lobes, the sound pressure simulated levels and positions are in fair agreement with the measurements.

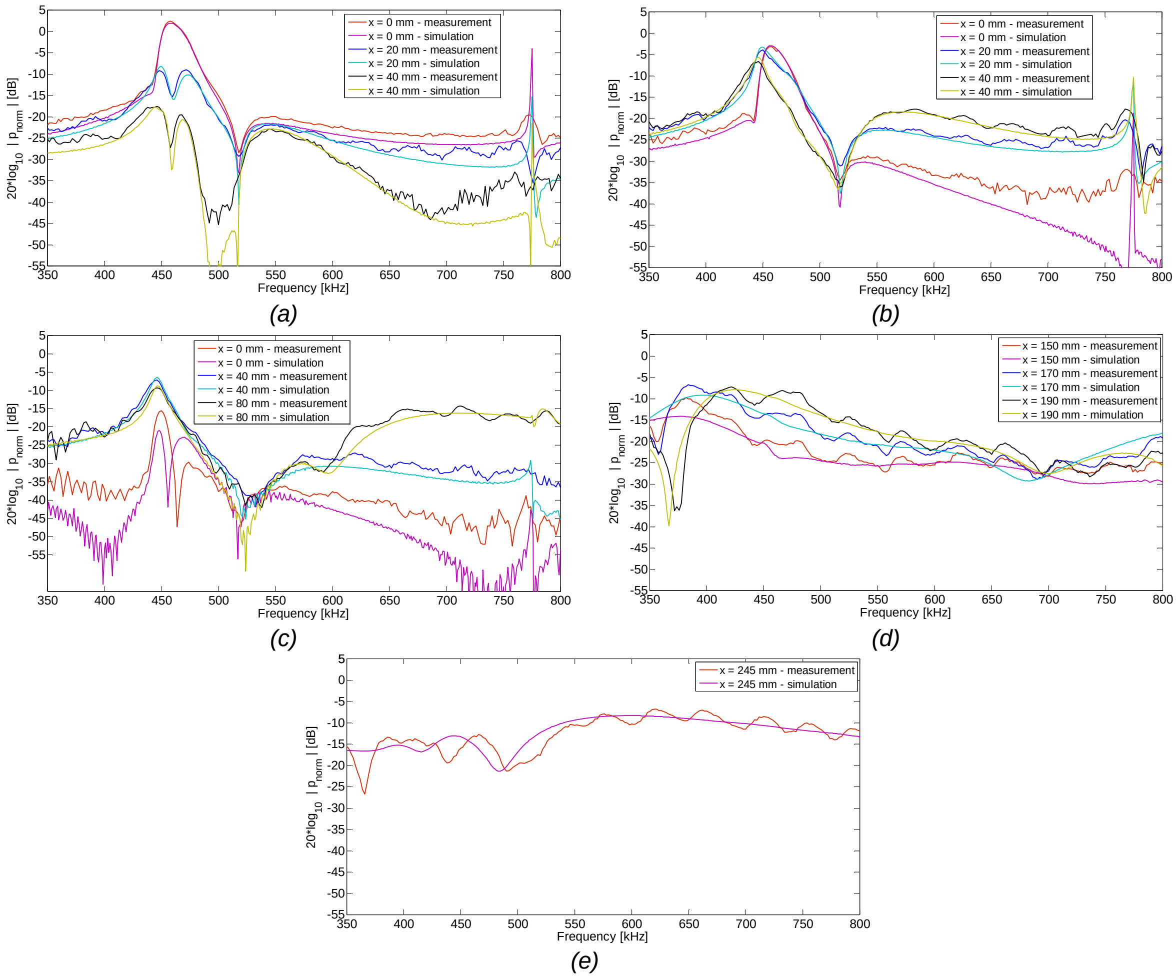

Figure 16. Measurement results and simulation results with 3D beam model of transmitted frequency spectra at z=376.05 mm and y=0 mm. (a) 0° incident angle, for x = 0 mm, x = 20 mm and x = 40 mm, (b) 5° incident angle, for x = 0 mm, x = 20 mm and x = 40 mm, (c) 10° incident angle, for x = 0 mm, x = 20 mm and x = 40 mm, (d) 25° incident angle, for x = 150 mm, x = 170 mm and x = 190 mm, (e) 30° incident angle, for x = 245 mm.

From the simulation and measurement results shown in Figure 16, it is found that the simulations using the 3D beam model are in a fair agreement with the measurement results. Close quantitative agreement is found at and around the S_1 and S_2 modes (350–700 kHz) in Figure 16 (a), at all three distances as shown. Close agreement is found in the lower part of the frequency responses (350–600 kHz) in Figure 16 (b), and fair agreement also in the upper part of the responses - especially at x = 20 and 40 mm. However, large deviation is found for x = 0 mm in the high frequency region. Close quantitative agreement is found in the lower part of the frequency responses (350–600 kHz) in Figure 16 (c), for x = 40 and 80 mm. Some "ripples" in the experimental measurements above 550 kHz can also be observed, and for x = 0 mm, the agreement is poor, the measurement is also influenced by noise and aliasing problems are found in the simulation result. Fair agreement is found of the frequency region investigated (350–800 kHz) in Figure 16 (d), at the distances x = 150, 170 and 190 mm. However, significant "ripples" is observed in the measurement results in the whole frequency range. Fair quantitative agreement is found in the whole frequency region (350–800 kHz) in

Figure 16 (e), at x = 245 mm. However, significant "ripples" is observed in the measurement results.

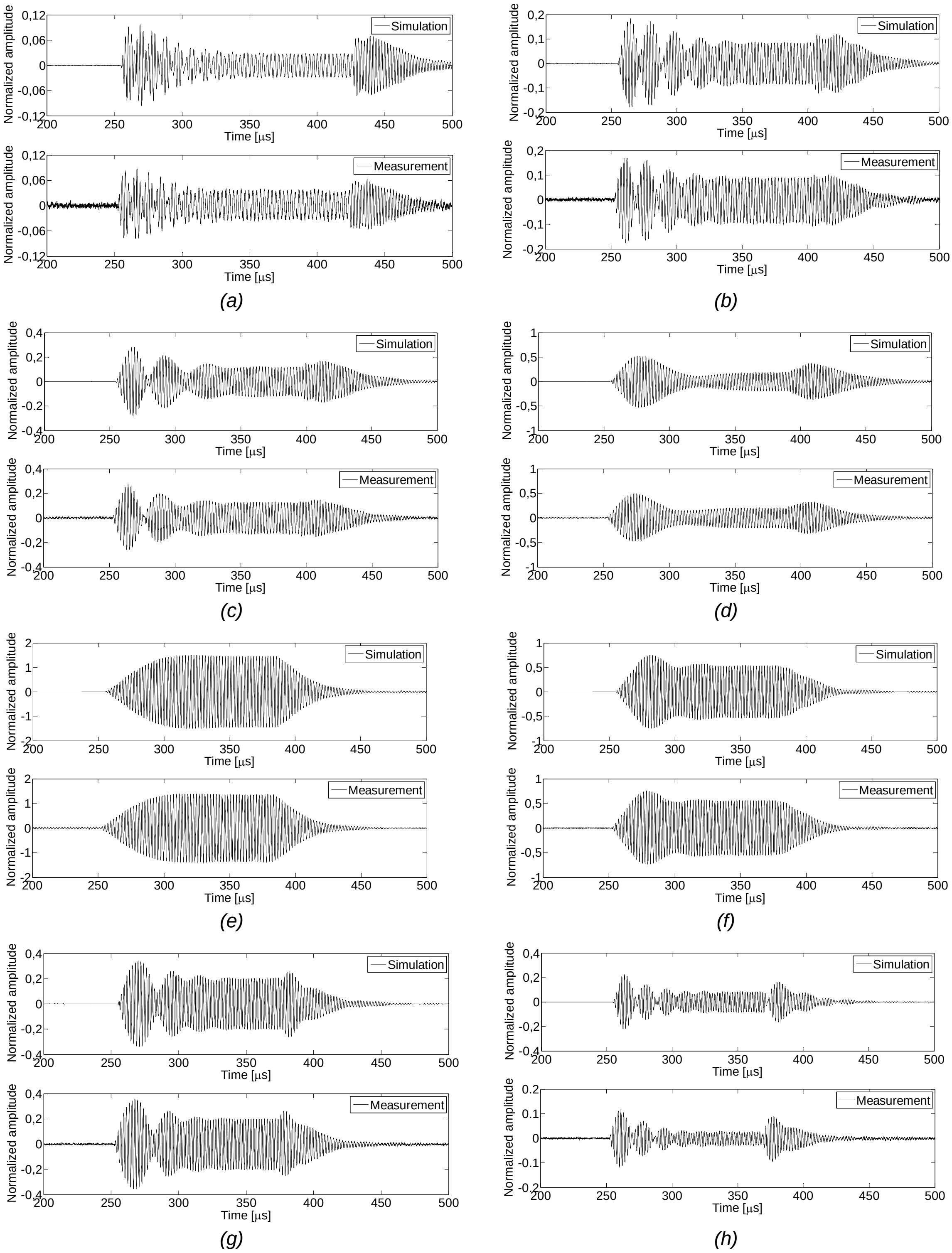

Figure 17. Measurement results and simulation results with 3D beam model of transmitted time-domain signals at 0° incident angle, at x=0 mm, and at z=376.05 mm. (a) 350 kHz, (b) 400 kHz, (c) 420 kHz, (d) 440 kHz, (e) 460 kHz, (f) 480 kHz, (g) 500 kHz, (h) 520 kHz.

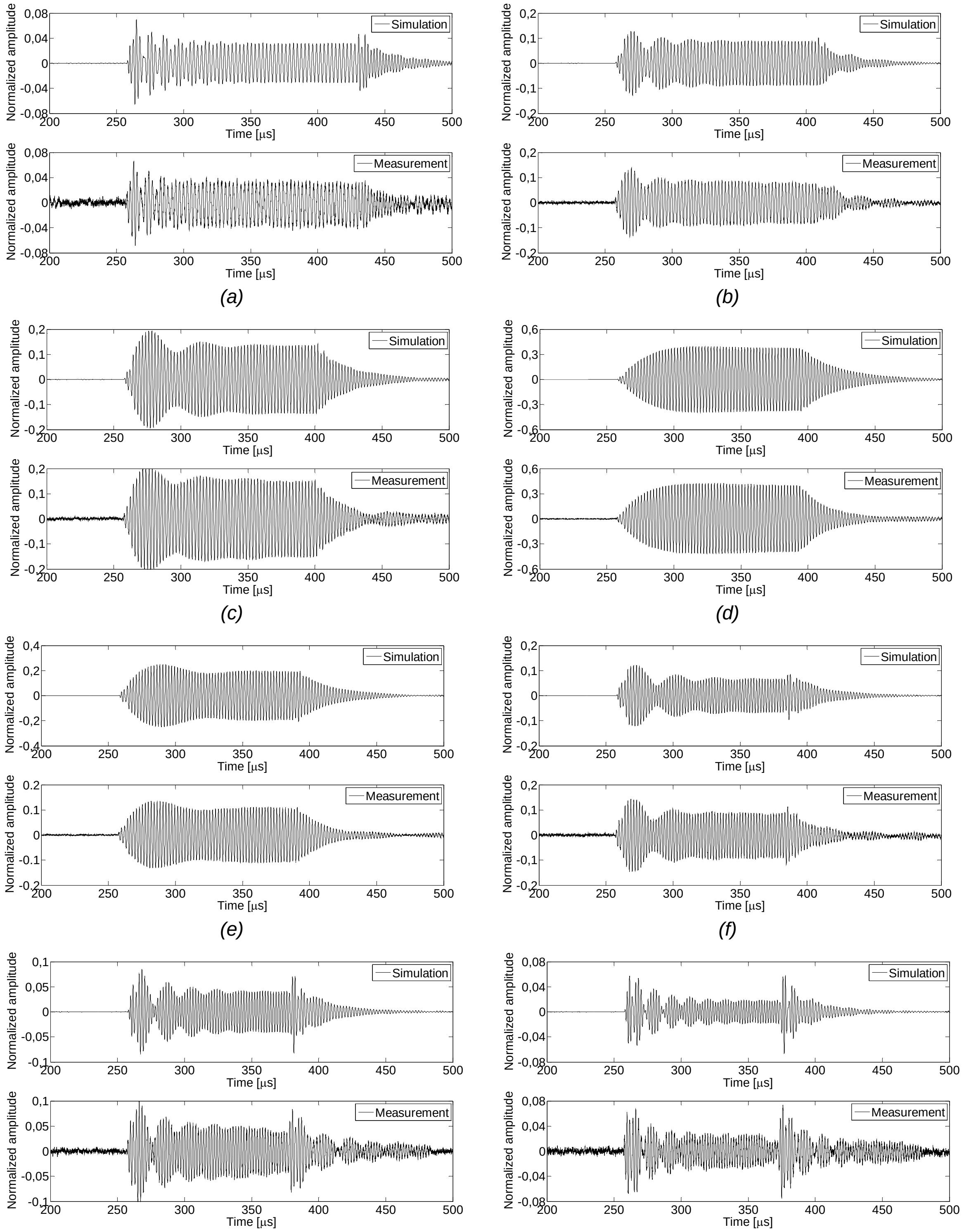

(g) (h)

Figure 18. Measurement results and simulation results with 3D beam model of transmitted time-domain signals at 10° incident angle, at x=60 mm, and at z=376.05 mm. (a) 350 kHz, (b) 400 kHz, (c) 420 kHz, (d) 440 kHz, (e) 460 kHz, (f) 480 kHz, (g) 500 kHz, (h) 520 kHz.

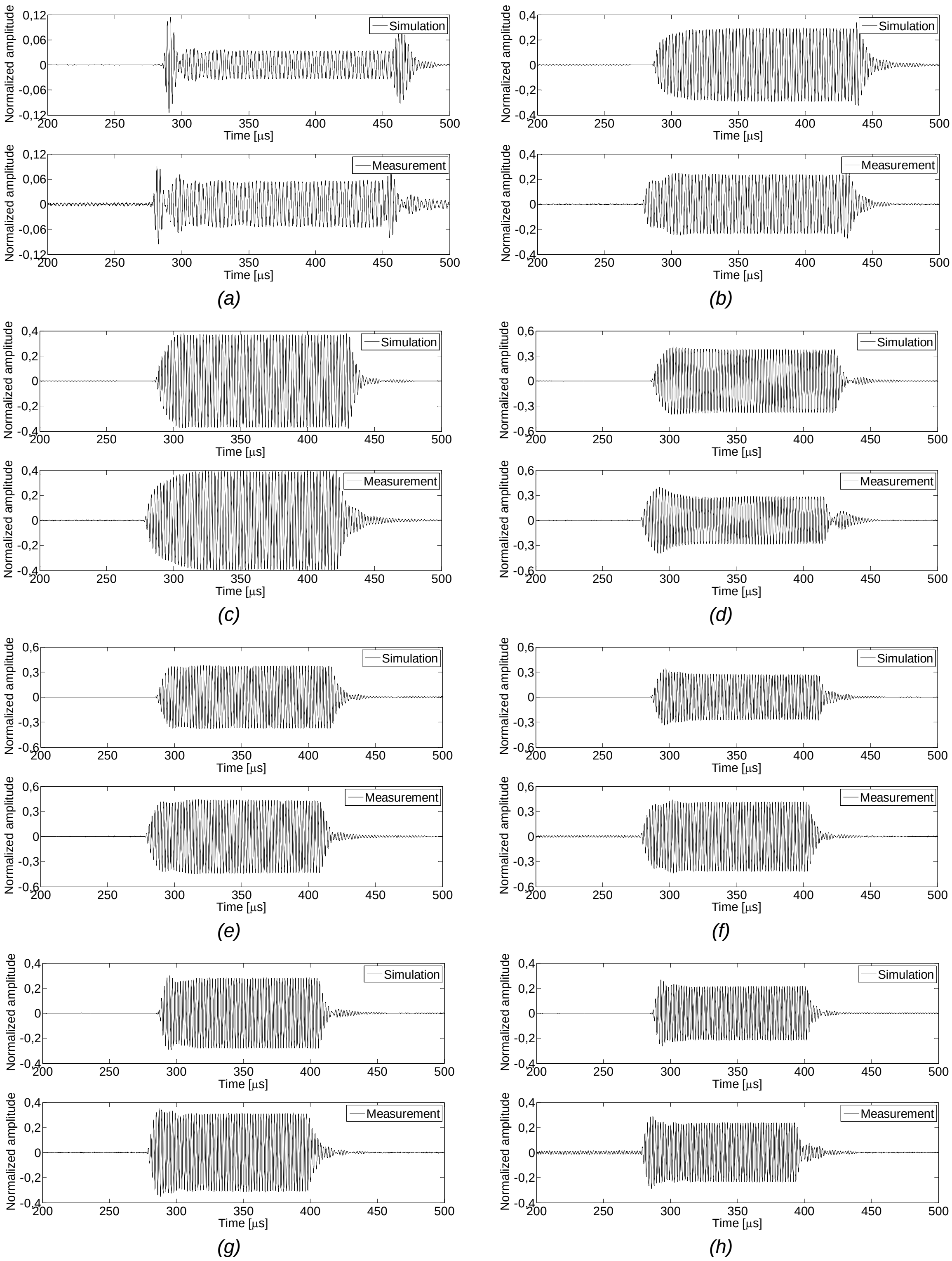

Figure 19. Measurement results and simulation results with 3D beam model of transmitted time-domain signals at 25° incident angle, at x=190 mm, and at z=376.05 mm. (a) 350 kHz, (b) 400 kHz, (c) 420 kHz, (d) 440 kHz, (e) 460 kHz, (f) 480 kHz, (g) 500 kHz, (h) 520 kHz.

In general, Figures 17 - 19 show a good correspondence between simulation results and measurement results of time-domain signals. The amplitudes and shapes of the time-domain signals in the simulations follow the measurement results fairly closely, for the frequencies and distances investigated, especially at 0° and 10° incidence. At 25° incidence, the simulations results differ somewhat when studying the level and a for some results also a little in the signal shape.

At 0° incidence, the signals in Figure 17 (e) and (h) are according to Figure 6 close to excitation of the S_1 and S_2 modes, respectively. Figure 17 (e) shows that the bandwidth for the S_1 mode is not large since the rise-time of the signal is long. This conclusion is also supported by the simulation in Figure 14 (a), and the measurement and simulation in Figure 16 (a).

At 10° incidence, the signals in Figure 18 (a) and (d) are according to Figure 6 close to excitation of the A_1 and S_1 modes, respectively. As shown in Figure 6, the A_1 mode is in this frequency region close to a region with very low transmission, and this may be the reason why the signal in Figure 18 (a) has a low level even if it is from plane wave theory believed that transmission at incident angles and frequencies generating Lamb waves in the plate should have resulted in maximum transmission. As shown in the simulation in Figure 14 (c) there is no maximum transmission due to the A_1 mode at 10° incidence. Figure 18 (d) shows that the bandwidth for the S_1 mode is not large since the rise-time of the signal is long. This conclusion is also supported by the simulation in Figure 14 (c), and the measurement and simulation in Figure 16 (c).

At 25° incidence, the signal in Figure 19 (d) corresponds to the excitation of the S_0 mode according to Figure 6. The signals in Figure 19 (a) - (h) show that the rise-time of the signals is relatively short, i.e. the bandwidth is relatively large. This conclusion is also supported by the simulation in Figure 14 (f) and Figure 16 (d) which shows that the S_0 mode has a larger bandwidth for beam excitation at x = 190 mm.

5. Discussion

To include the effects from the side lobes which are present for most real transducers, it is important to model the transducer as a directive piston source which generates a 3D directive piston source field instead of a transducer which generates a 2D Gaussian beam. However, to get accurate results from the 3D beam model; the directive piston source field must be representative for the transducer in the experimental setup. If this is the case, then the piston model can be used in the 3D beam model. However if this is not true, then it may e.g. be possible to measure the directivity for the transducer for several frequencies and use this as input into the 3D beam model. This is however a demanding and slow process. Another approach is to simulate the directivity of the transducer with e.g. a finite element model and use the simulation result as input to the 3D beam model.

The measured directivity for the transmitting transducer in the measurement setup here was compared to simulation results with the piston model in Section 4.2. The results showed fairly good agreement between the measured and simulated directivity; thus the piston model may be considered to be a fairly good model for the transmitter transducer used in the experimental setup. The side lobes are however not accurately described by the piston model, which may affect the simulation results as compared to the measurements. A piston source may give a fairly good description of the transmitter transducer, as shown here, but a finite element simulation of the beam from the transmitter transducer can be more accurate.

Comparisons between measurements and 3D simulation results of the transmission through the water-immersed steel plate have shown a fairly good correspondence in space-time and frequency-space domains for various frequencies and incident angles as shown in Figures 15 - 19, but some oscillations are observed in the measurements for large incident angles. The reason for these oscillations and hence the mismatch to the 3D simulation results might be due to the experimental setup, i.e. for transmission measurements at oblique incident angles and the hydrophone in the experimental setup has been moved to different x-positions without rotating around it's axis and hence the front face of the hydrophone is only perpendicular to the transmitted beam at normal incidence.

However, at normal incidence as was shown in Figure 8, the normalization method reduced the oscillations/interference in the raw transmission measurements above 525 kHz. It has not been tested if the interferences in the measurements in water also are reduced (as shown in Figure 7) if the beam from the transducer is not normal incident towards the front face of the hydrophone. Other factors that might result in differences between measurement results and simulation results are that the fluid (water) and solid (steel-plate) have been modelled as loss-less in the 3D beam model, the side lobes are not accurately described with the piston model and the steel plate is not infinitely large, thus and especially at large incidences, reflections from the edge of the plate may be present.

For the measurement setup studied, the 3D beam model presented and used here is considered to give a fairly realistic representation of the system involving a steel plate immersed in water although the fluid (water) and solid (steel-plate) have been modelled as loss-less in the 3D beam model. The general fair-to-close agreement between the 3D beam simulations and the measurement results shown in Figures 15 – 19 gives confidence to the 3D beam simulation results such as shown in Figure 14. Thus, the simulation results presented in Figure 14 may be useful for choosing e.g. the incident angle etc. for obtaining high transmission level and high bandwidth, and the 3D beam model may increases the knowledge and understanding of how the transmission develops at different incident angles. With respect to acoustic properties for a water-immersed steel plate as investigated here, the simulation results in Figure 14 can be used for studying bandwidth, signal-level and directivity, while the pulse-form can be studied with simulation results as shown in Figures 17 – 19. From Figure 14, it is noted that the transmitted signal level is largest when exciting the S_1 mode at normal incidence, while the bandwidth and directivity is narrow. It is also noted from the incident angles investigated in Figure 14 that the transmitted bandwidth is largest when transmission through the plate is carried out with an incident angle and a frequency range which corresponds to excitation of S_0 and A_0 modes, or a combination of these modes. In addition to signal level and bandwidth, the plots in Figure 14 show the directivity in the x-direction. From the simulation results with the 3D beam model, it is also possible to plot similar plot as in Figure 14 as a function of y-direction.

Since the simulations with the 3D beam model give a fairly good description of the measurements, an extension of the 3D beam model to include different media at the plate's interfaces (and e.g. in combination with a finite element model to include better transducer response) may be used as a tool for developing and optimizing apparatus where transmission of ultrasonic directive beams through a plate or a pipe wall.

Measurements and simulations with plane wave and 3D beam models of the transmission at normal incidence have shown that the shear velocity for the steel plate can be estimated by using a combination of plane wave and 3D beam model simulations. However, the results have also shown that the longitudinal velocity for the steel plate can not be determined by using the plane wave model in combination with the measured transmitted frequency response for all longitudinal resonance frequencies. As has been shown for the S_1 mode at normal incidence, the maximum of the measured transmission does not always correspond to the cut-off frequencies calculated with the plan wave model. The possible reason for this mismatch for the S_1 mode might be due to the nature of this mode as shown in Figure 6, i.e. for small incident angles, this mode is excited in the plate at lower frequencies then at normal incidence. Hence, a normal incident beam will possibly also excite this mode at small incident angles and this may shift the cut-off frequency to a lower frequency compared to a plane wave normal incident sound field. However, the 3D beam model has shown fairly good correspondence also for this longitudinal mode at normal incidence. Measurements and comparison to plane wave simulation results at higher frequencies where the beam is more narrow and where the mode does not have this characteristic behaviour around normal incidence, have given better correspondence (shown in Figures 9 and 10, and in [21]).

6. Conclusions

In this work, a 3D beam model for the reflection and transmission of 3D directive beams from and through a fluid-immersed solid plate has been implemented and compared with experimental measurements in the space-time and frequency-space domains, and a fairly good correspondence is shown. The shear wave velocity has been determined using transmitted pressure frequency response measurements combined with plane wave and 3D simulations, and measurements at normal incidence have been used to determine both the longitudinal and shear wave velocities.

The normalization method used here has been beneficial in the measurements since it has reduced the interference problem from the hydrophone when using long sinusoidal excitation signals. The normalization method has also made it possible to compare 3D simulation results with measurements at different frequencies at the same level, so that the transmission obtained with a frequency where the signal level from the transducer is weak, can directly be compared with results when exciting the transducer at the resonance frequency.

Acknowledgements

The present work has been supported by The Research Council of Norway (NFR) under the 4-year KMB/Petromaks project "New subsea and downhole instrumentation", in a cooperation between Statoil, the University of Bergen and Christian Michelsen Research AS (CMR). The present work is made as a part of the PhD work of the first author, under Task 4 of the KMB/Petromaks project; "Subsea allocation and fiscal measurement". Contributions from Stig Heggstad (CMR), Reidar Bø (CMR) and Kåre Slettebakken (UoB) on the design and construction of the measurement setup, and from Gaute Lied (CMR) on the development of the Soundfield software for acquisition and processing of measurement signals, and steering of the hydrophone scanning systems, are highly acknowledged.

References

[1] Bertoni, H. L. and Tamir, T., 1973, Unified theory of rayleigh-angle phenomena for acoustic beams at liquid-solid interfaces, Applied Physics A: Material Science & Processing **2** (4), 157-172.

[2] Breazeale, M. A., Adler, L. and Scott, G. W., 1977, Interaction of ultrasonic waves incident at the Rayleigh angle onto a liquid-solid interface, Journal of Applied Physics **48**, 530-537.

[3] Pitts, L. E., Plona, T. J. and Mayer, W. G., 1976, Ultrasonic bounded beam reflection and transmission effects at a liquid/solid-plate/liquid interface, The Journal of the Acoustical Society of America **59** (6), 1324-1328.

[4] Pitts, L. E., Plona, T. J. and Mayer, W. G., 1977, Theory of nonspecular reflection. effects for an ultrasonic beam incident on a solid plate in a liquid, IEEE Transactions on Sonics and Ultrasonics **24** (2), 101-108.

[5] Ng, K. W., 1979, Non-specular ultrasonic bounded beam transmission through solid plates, PhD thesis, Georgetown University, Physics Department, Washington DC, United States.

[6] Ngoc, T. D. and Mayer, W., 1980, A general description of ultrasonic nonspecular reflection and transmission effects for layered media, IEEE Transaction on Sonics and Ultrasonics **27** (5), 229-236,.

[7] Ngoc, T. D. and Mayer, W. G., 1980, Numerical integration method for reflected beam profiles near Rayleigh angle, The Journal of the Acoustical Society of America **67** (4), 1149-1152.

[8] Schmidt, H., and Jensen, F. B., 1985, A full wave solution for propagation in multilayered viscoelastic media with application to Gaussian beam reflection at fluid-solid interfaces, The Journal of the Acoustical Society of America **77** (3), 813-825.

[9] Chimenti, D. E., Zhang, J. G., Zeroug, S. AND Felsen, L. B., 1994, Interaction of acoustic beams with fluid-loaded structures, The Journal of the Acoustical Society of America **95** (1), 45-59.

[10] Landsberger, B. J., 1997, Second harmonic generation in sound beams reflected from and transmitted through immersed elastic solids, PhD thesis, University of Texas, Austin, United States.

[11] Landsberger, B. J. and Hamilton, M. F., 2001, Second harmonic generation in sound beams reflected from, and transmitted through, immersed elastic solids, The Journal of the Acoustical Society of America **109** (2), 488-500.

[12] Younghouse, S. J., 2002, Irradiation of an elastic plate by a finite-amplitude sound beam with applications to nondestructive evaluation, PhD thesis, University of Texas, Austin, United States.

[13] Rayleigh, L., 1888-1889. *On the free vibrations of an infinite plate of homogeneous isotropic matter*, Proc. of the London Math. Soc., 20, 225-234.

[14] Lamb, H., 1889-1890. *On the flexure of an elastic plate,* Proc. of the London Math. Soc., 21, 70-91.

[15] Lamb, H., 1917. *On waves in an elastic plate,* Proc. *of the Roy. Soc. of London*, 93, 114-128.

[16] Rose, J. L., 1999. *Ultrasonic waves in solid media.* (Cambridge University Press).

[17] Lowe, M. J., 1993. *Plate waves for the NDT of diffusion bonded titanum*, (PhD thesis at Dept. of Mech. Eng., Imperial College of Science, Technology and Medicine, London).

[18] Brekhovskikh, L. M., 1980. *Waves in layered media.* (Academic press INC, San Diego, California).

[19] Schmerr, L. W. JR., 1998, *Fundamentals of ultrasonic nondestructive evaluation. A modeling approach*, (Plenum Press, New York).

[20] Matweb, http://www.matweb.com/search/DataSheet.aspx?MatID=12803&ckck=1 , (2008).

[21] Lohne, K. D., *Transmission of 3-D ultrasonic directive beams through a water immersed steel plate. Experimental and simulation results*, PhD thesis, Department of Physics and Technology, University of Bergen, In preparation.